 CMES, vol.31, no.3, pp.145-156, 2008

A Meshless Local Natural Neighbour Interpolation Method Applied to Structural Dynamic Analysis

Y. H. Liu[1,2], S. S. Chen[1], J. Li[1] and Z. Z. Cen[1]

Abstract: A novel meshless method for structural dynamic analysis is presented and discussed in this paper. It is called meshless local natural neighbour interpolation (MLNNI) method, which uses a meshless spatial approximation based only on nodes. The MLNNI is derived from the generalized meshless local Petrov-Galerkin (MLPG) method as a special case. Local weak forms are developed using weighted residual method locally from the dynamic partial differential equation. In the construction of trial functions, the natural neighbour interpolation (NNI) is employed to simplify the treatment of the essential boundary conditions. The domain integration is evaluated over included Delaunay triangles in each polygonal subdomain. The validity and strength of the proposed method for free and forced vibration analyses are demonstrated throughout different numerical applications. It is proven from the results that the proposed method is quite easy to implement, very accurate and highly efficient for both free vibration analysis and forced vibration analysis.

Keyword: Meshless method, MLPG, Natural neighbour interpolation, Free/forced vibration analysis, Newmark method

1 Introduction

Structural dynamic analysis is one of the main required tasks for an engineer to accomplish in the engineering design. These dynamic problems are classically described by a linear partial differential equation associated with a set of boundary conditions and initial conditions. Analytical solutions to these boundary value and initial value problems are usually very limited. In addition, their derivations generally need simplifications and the resultant accuracy is therefore sacrificed. Therefore, the dynamic analysis of solids and structures can practically be treated only by numerical methods. Among the various numerical methods, the finite element method (FEM) has been successfully used in most cases. However in the case of complex geometries the generation of highly distorted meshes is common. The distortion of meshes causes low quality shape functions which can affect the performance of the method.

In recent years, more and more attention is paid to the development and application of meshless methods. In principle, meshless methods rely only on a group of scattered nodes in the problem domain, which can not only alleviate the burdensome to generate mesh, but also describe more accurately the irregular geometries. Some meshless methods are based on the global weak forms, such as the smooth particle hydrodynamics (SPH) by Gingold and Moraghan (1977), the element-free Galerkin (EFG) method by Belytschko et al. (1994) and the reproducing kernel particle method (RKPM) by Liu et al. (1995). They still require a mesh of background cells for integration in computing the system matrices, and so they are "meshless" only in terms of the interpolation of the field or boundary variables. Pursuit of truly meshless methods therefore continues. The meshless local Petrov-Galerkin (MLPG) method originated by Atluri and Zhu (1998) starts from a local weak form and satisfies governing equation node-by-node in a local way of making weighted residual zero over a subdomain. Integration of the weak form is performed in local subdomains with simple geometrical shapes and therefore no ele-

[1] Department of Engineering Mechanics, School of Aerospace, Tsinghua University, Beijing 100084, P. R. China

[2] Corresponding author. Tel: +86-10-62773751; fax: +86-10-62781824; Email: yhliu@mail.tsinghua.edu.cn

ments or background cells are required either for interpolation purposes or for integration purposes. By now, the MLPG method has been successfully applied in analyzing 3D problems in elastostatics [Han and Atluri (2004)], nonlinear problems with large deformations and rotations [Han, Rajendran and Atluri (2005)], high-speed impact, penetration and perforation problems [Han et al. (2006)], magnetic diffusion [Johnson and Owen (2007)], limit analysis [Chen, Liu and Cen (2008)], etc. Furthermore, the MLPG method enables us to construct various meshless approaches easily by different choices and combinations of the trial and test functions [Atluri, Kim and Cho (1999)]. Up to now, many meshless approaches have been developed based on the concept of MLPG [De and Bathe (2000), Liu and Gu (2001), Barry (2004), Xiao (2004), Li, Wang and Lam (2004), Cai and Zhu (2004), Wang, Zhou and Shan (2005)]. Among these, the meshless local natural neighbour interpolation (MLNNI) method [Cai and Zhu (2004)] shows great promise since it can not only maintain prominent features of the MLPG method but also employ the advantage of easy imposition of essential boundary conditions of the natural neighbour interpolation (NNI).

The NNI is a multivariable interpolation scheme based on Voronoi diagram of scattered nodes. This interpolation scheme has been successfully applied in natural element method [Sukumar, Moran and Belytschko (1998)] and natural neighbour Galerkin method [Sukumar, Moran, Semenov and Belikov (2001)]. The NNI function passes exactly through the nodal values and the essential boundary conditions can be directly imposed on the nodes. The NNI also exhibits other distinct and attractive features, such as optimum spatial adjacency, desirable smoothness and well-defined approximation without uncertain user-defined parameters. Furthermore, the computation of the shape functions with this method is very simple and needs much less numerical effort than in the moving least squares approximation [Most (2007)]. Consequently, the NNI appears to be a good choice for constructing trial functions in the MLNNI.

In this paper, attention will be devoted to the MLNNI formulations for free and forced vibration analyses of two-dimensional solids and structures. Local weak forms are developed using weighted residual method locally from the dynamic partial differential equation. The natural neighbour interpolation is employed to construct meshless shape functions for a set of randomly distributed nodes, and the three-node triangular FEM shape functions are used as test functions. The Delaunay tessellation is used to construct the local subdomains, which have polygonal shapes and are coincident with the supports of nodal test functions. The shape functions formed satisfy the delta function property, so the imposition of the essential boundary conditions is easy. Frequencies and eigenmodes of free vibration are obtained by solving an eigenvalue equation and the forced vibration system equation is solved numerically by the Newmark method as a time stepping method. Finally, several numerical problems are studied to demonstrate the validity and accuracy of the proposed method.

2 Natural Neighbour Interpolation

In order to reduce the computational cost and simplify the imposition of the essential boundary conditions, the natural neighbour interpolation (NNI) is employed for constructing trial functions in the present study. It relies on the concepts of Voronoi diagram of the given cloud of nodes and its dual Delaunay tessellation. Each Voronoi cell represents the space closet to a given node. Thus, a first-order Voronoi diagram for a set of nodes $\mathbf{N} = \{\mathbf{x}_1, \ \mathbf{x}_2, \ \mathbf{x}_3, \ \cdots, \ \mathbf{x}_M\} \in R^2$ is a subdivision of the space into sub-regions T_I such that any point $\mathbf{x}$ in T_I is closer to node $\mathbf{x}_I$ than to any other node in the domain [Green and Sibson (1978)],

$$T_I = \{\mathbf{x} \in R^2 \ : \ d(\mathbf{x}, \mathbf{x}_I) < d(\mathbf{x}, \mathbf{x}_J) \quad \forall J \neq I\} \quad (1)$$

where $d(\mathbf{x}, \mathbf{x}_I)$ is the distance between $\mathbf{x}$ and $\mathbf{x}_I$. The Delaunay triangulation is the geometrical dual of the Voronoi diagram and it is constructed by connecting the nodes whose Voronoi cells have common boundaries. For the definition of Sibson interpolation it is necessary to previously introduce the concept of second-order Voronoi cell. It

is defined as the locus of the points that have the node $\mathbf{x}_I$ as the closet node and the node $\mathbf{x}_J$ as the second closet node:

$$T_{IJ} = \{\mathbf{x} \in R^2 \,:\, d(\mathbf{x},\mathbf{x}_I) < d(\mathbf{x},\mathbf{x}_J) < d(\mathbf{x},\mathbf{x}_K) \quad \forall J \neq I \neq K\} \quad (2)$$

T_{IJ} is non-empty only if $\mathbf{x}_I$ and $\mathbf{x}_J$ are natural neighbours. The natural neighbour shape functions of $\mathbf{x}$ with respect to the node $\mathbf{x}_I$ are defined in two dimensions as the ratio of the area of T_{xI} and T_x

$$\phi_I(\mathbf{x}) = A_I(\mathbf{x})/A(\mathbf{x}) \quad (3)$$

where

$$A(\mathbf{x}) = \sum_{J=1}^{n} A_J(\mathbf{x}) \quad (4)$$

and n is the number of natural neighbours of the point $\mathbf{x}$. Referring to Figure 1, the shape function $\phi_1(\mathbf{x})$ may be represented as

$$\phi_1(\mathbf{x}) = A_{abfe}/A_{abcd} \quad (5)$$

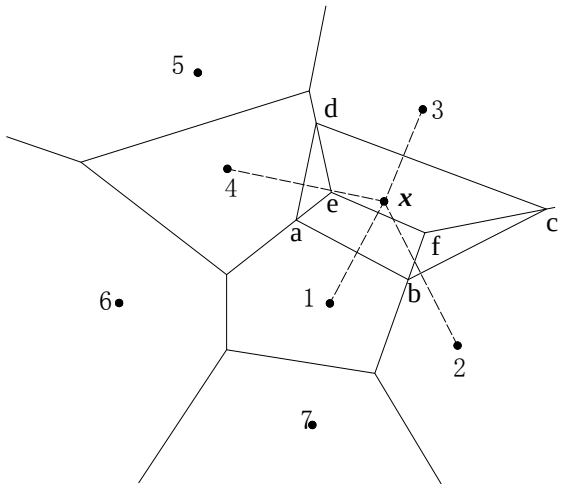

Figure 1: 1st-order and 2nd-order Voronoi cells about $\mathbf{x}$

From this definition, and in the context of two-dimensional approximations, the unknown displacement field $\mathbf{u}(\mathbf{x})$ is approximated in the form

$$\mathbf{u}^h(\mathbf{x}) = \sum_{I=1}^{n} \phi_I(\mathbf{x})\mathbf{u}_I \quad (6)$$

where $\mathbf{u}_I$ is the vector of nodal displacements of the n natural neighbours of the point $\mathbf{x}$.

It is straightforward to prove that the NNI shape functions form the properties of positivity, interpolation, and partition of unity [Sukumar, Moran and Belytschko (1998)]:

$$0 \leq \phi_I(\mathbf{x}) \leq 1,\ \phi_I(\mathbf{x}_J) = \delta_{IJ},\ \sum_{\mathrm{I}=1}^{n} \phi_I(\mathbf{x}) = 1 \quad (7)$$

The NNI shape functions also satisfy the local coordinate property, namely

$$\mathbf{x} = \sum_{I=1}^{n} \phi_I(\mathbf{x})\mathbf{x}_I \quad (8)$$

which, in conjunction with Eq. (7) imply that the NNI spans the space of linear polynomials (linear completeness). Furthermore, the NNI shape functions have C^∞ continuity everywhere, except at the nodes where they areC^0. Importantly, the NNI shape functions have delta function property while the shape functions derived from the moving least squares approximation lack this property. Hence, the advantage of the NNI is attractive for practical applications.

3 Formulation of the MLNNI method for dynamic simulation

3.1 Basic equations of elastodynamics

In two-dimensional problems with small displacements in the domain Ω bounded by Γ_u and Γ_t, the governing equation for structural dynamics is:

$$\sigma_{ij,j} + b_i = \rho\ddot{u}_i + c\dot{u}_i \text{ in } \Omega \quad (9)$$

where ρ is the mass density, c is the damping coefficient, $\ddot{u}_i = \partial^2 u_i/\partial t^2$ is the acceleration, $\dot{u}_i = \partial u_i/\partial t$ is the velocity, σ_{ij} is the stress tensor corresponding to the displacement u_i, b_i is the body force, and $(\,)_{,j}$ denotes $\partial/\partial x_j$. The corresponding boundary and initial conditions are given as follows:

$$u_i = \overline{u}_i \text{ on the essential boundary } \Gamma_u, \quad (10a)$$

$$\sigma_{ij}n_j = \overline{t}_i \text{ on the natural boundary } \Gamma_t, \quad (10b)$$

$$\mathbf{u}(\mathbf{x},t_0) = \mathbf{u}_0(\mathbf{x}), \text{ displacement initial condition,}$$

(10c)

$$\dot{\mathbf{u}}(\mathbf{x},t_0)=\mathbf{v}_0(\mathbf{x}),\ \text{velocity initial condition} \quad (10d)$$

where $\overline{u}_i$, $\overline{t}_i$, $\mathbf{u}_0$ and $\mathbf{v}_0$ denote the prescribed displacements, tractions, initial displacements and velocities, respectively, and n_j is the unit outward normal vector to the boundary Γ.

3.2 Free vibration

When b_i and c in Eq. (9) are set equal to zero, the governing equation for no damping free vibration can be written as

$$\rho\ddot{u}_i-\sigma_{ij,j}=0. \quad (11)$$

The boundary conditions are usually the same form of Eq. (10a) and Eq. (10b), but the traction $\overline{t}_i=0$. For the free vibration problems with the natural circle frequency ω, $u(\mathbf{x},t)$ can be written as follows:

$$u(\mathbf{x},t)=u(\mathbf{x})\sin(\omega t+\varphi) \quad (12)$$

Substituting Eq. (12) into Eq. (11) leads to the following differential equation for free vibration of an isotropic homogeneous elastic body:

$$\sigma_{ij,j}+\omega^2\rho u_i=0 \quad (13)$$

In the MLNNI method a weak form over the local subdomains such as Ω_s is constructed. The local subdomain is a small region taken for each node inside the global domain. They can be overlapping each other, and cover the whole global domainΩ. Because the NNI shape functions have the delta function property, the essential boundary conditions can be imposed directly. Using the local weighted residual technique, the local weak form of Eq. (13) can be written as

$$\int_{\Omega_s}v_i(\sigma_{ij,j}+\omega^2\rho u_i)\mathrm{d}\Omega=0, \quad (14)$$

where v_i is the test function.

Using the relationship

$$v_i\sigma_{ij,j}=(v_i\sigma_{ij})_{,j}-v_{i,j}\sigma_{ij} \quad (15)$$

and the divergence theorem in Eq. (14) leads to

$$\int_{\Gamma_s}v_i\sigma_{ij}n_j\mathrm{d}\Gamma-\int_{\Omega_s}(v_{i,j}\sigma_{ij}-v_i\omega^2\rho u_i)\mathrm{d}\Omega=0. \quad (16)$$

The support subdomain Ω_s of node $\mathbf{x}_I$ is a domain in which $v_i(\mathbf{x})\neq 0$. When there is an intersection between the local boundary Γ_s and the global boundary Γ, the boundary Γ_s is usually composed of three parts: the internal boundary Γ_{sI}, the boundaries Γ_{su} and Γ_{st} over which the essential and natural boundary conditions are specified. If there is no intersection between Γ_s and the global boundary Γ, $\Gamma_{sI}=\Gamma_s$. Imposing the natural boundary condition and noticing that $\sigma_{ij}n_j=t_i$, Eq. (16) can be rewritten as

$$\int_{\Gamma_{sI}}v_it_i\mathrm{d}\Gamma+\int_{\Gamma_{su}}v_it_i\mathrm{d}\Gamma+\int_{\Gamma_{st}}v_it_i\mathrm{d}\Gamma-\int_{\Omega_s}(v_{i,j}\sigma_{ij}-v_i\omega^2\rho u_i)\mathrm{d}\Omega=0. \quad (17)$$

In the present analysis of free vibration, the integrals over Γ_{st} vanish for all nodes because of $\overline{t}_i=0$ on Γ_t. Therefore, Eq. (17) can be simplified as

$$\int_{\Gamma_{sI}}v_it_i\mathrm{d}\Gamma+\int_{\Gamma_{su}}v_it_i\mathrm{d}\Gamma-\int_{\Omega_s}(v_{i,j}\sigma_{ij}-v_i\omega^2\rho u_i)\mathrm{d}\Omega=0 \quad (18)$$

In the MLNNI method, as trial functions are constructed by the NNI, which is based on the Delaunay tessellations, it is natural to construct polygonal subdomain Ω_s using the Delaunay tessellations. Therefore the polygonal subdomain Ω_s corresponding to node $\mathbf{x}_I$ is constructed by collecting all the surrounding Delaunay triangles T_{iI} with node $\mathbf{x}_I$ being their common vertices, as shown in Figure 2. By choosing the test functions v_i to be the three-node triangular FEM shape functions N_I in each Delaunay triangle T_{iI} belonging to the subdomain Ω_s centered at node $\mathbf{x}_I$, we obtain the following local weak form:

$$\int_{\Gamma_{su}}v_it_i\mathrm{d}\Gamma-\int_{\Omega_s}(v_{i,j}\sigma_{ij}-v_i\omega^2\rho u_i)\mathrm{d}\Omega=0 \quad (19)$$

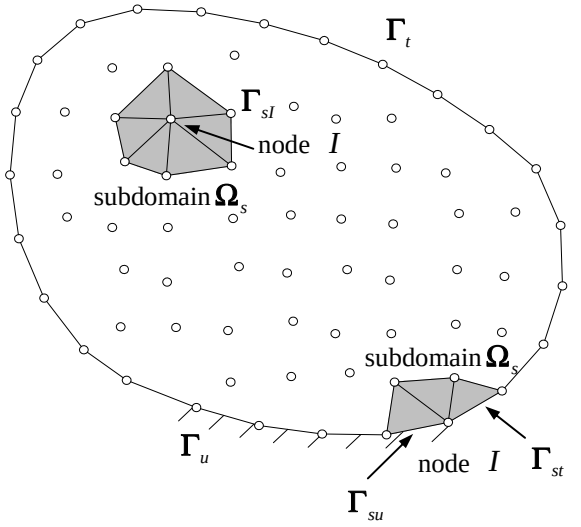

Figure 2: Local polygonal subdomain and boundary for node I

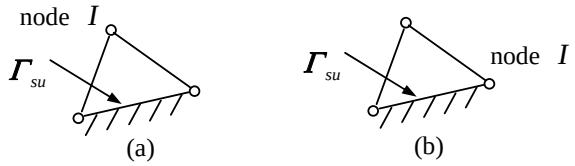

Figure 3: Essential boundary condition Γ over subdomain Ω_s

It should be noted that the integrals over Γ_{su} in Eq. (19) can be divided into two cases as shown in Figure 3. For Figure 3a, the test functions N_I are equal to zero over the local prescribed boundary Γ_{su}, and the integrals over Γ_{su} are also equal to zero; For Figure 3b, although neither the reaction force t_i nor the test function N_I is zero, the corresponding stiffness item will vanish because of the restriction of prescribed displacements over Γ_{su}. Accordingly, Eq. (19) can be simplified as

$$\int_{\Omega_s} (v_{i,j}\sigma_{ij} - v_i\omega^2\rho u_i)\mathrm{d}\Omega = 0 \tag{20}$$

Substitution of Eq. (6) into the weak form (20) for all nodes leads to the following discretized system equation

$$(\mathbf{K} - \omega^2\mathbf{M})\mathbf{u} = 0, \tag{21}$$

where $\mathbf{u}$ is the eigenvector, $\mathbf{K}$ and $\mathbf{M}$ are the stiffness and mass matrices, respectively. They are derived in the following forms

$$\mathbf{K}_{IJ} = \sum_{i=1}^{M} \int_{T_{iI}} \mathbf{V}_I^{\mathrm{T}} \mathbf{D} \mathbf{B}_J \mathrm{d}\Omega \tag{21a}$$

$$\mathbf{M}_{IJ} = \sum_{i=1}^{M} \int_{T_{iI}} \rho N_I \mathbf{\Phi}_J \mathrm{d}\Omega \tag{21b}$$

where M is the total number of Delaunay triangles T_{iI} in the subdomain Ω_s centered at node $\mathbf{x}_I$, and other matrices are given as follows:

$$\mathbf{D} = \frac{E}{1-v^2}\begin{bmatrix} 1 & v & 0 \\ v & 1 & 0 \\ 0 & 0 & \frac{1-v}{2} \end{bmatrix} \text{ for plane stress,} \tag{22a}$$

$$\mathbf{V}_I = \begin{bmatrix} N_{I,x} & 0 \\ 0 & N_{I,y} \\ N_{I,y} & N_{I,x} \end{bmatrix}, \tag{22b}$$

$$\mathbf{B}_J = \begin{bmatrix} \phi_{I,x} & 0 \\ 0 & \phi_{I,y} \\ \phi_{I,y} & \phi_{I,x} \end{bmatrix}, \tag{22c}$$

$$\mathbf{\Phi}_J = \begin{bmatrix} \phi_J & 0 \\ 0 & \phi_J \end{bmatrix}. \tag{22d}$$

where E and v are the Young's modulus and Poisson's ratio, respectively.

Thus, the frequencies and modes of the free vibration can be computed by solving a linear eigenvalue problem Eq. (21).

3.3 Forced vibration

The governing equation, boundary and initial conditions for the forced vibration are presented in Eqs. (9) and (10a)-(10d). A local weak form of the partial differential Eq. (9), over a local domain Ω_s bounded by Γ_s, can be obtained using the local weighted residual technique

$$\int_{\Omega_s} v_i(\sigma_{ij,j} + b_i - \rho\ddot{u}_i - c\dot{u}_i)\mathrm{d}\Omega = 0, \tag{23}$$

Integrating the first term on the left-hand side of Eq. (23) by parts and imposing the natural boundary condition (10b), we have

$$\int_{\Omega_s} (v_i\rho\ddot{u}_i + v_i c\dot{u}_i + v_{i,j}\sigma_{ij})\mathrm{d}\Omega - \int_{\Gamma_{sI}} v_i t_i \mathrm{d}\Gamma - \int_{\Gamma_{su}} v_i t_i \mathrm{d}\Gamma = \int_{\Gamma_{st}} v_i \bar{t}_i \mathrm{d}\Gamma + \int_{\Omega_s} v_i b_i \mathrm{d}\Omega. \tag{24}$$

After some manipulations as described in Section 3.1, Eq. (24) can be simplified as

$$\int_{\Omega_s}(v_i\rho\ddot{u}_i+v_ic\dot{u}_i+v_{i,j}\sigma_{ij})\mathrm{d}\Omega = \int_{\Gamma_{st}}v_i\bar{t}_i\mathrm{d}\Gamma+\int_{\Omega_s}v_ib_i\mathrm{d}\Omega. \quad (25)$$

In the discretization of the local weak form of the forced vibration, approximation function $\mathbf{u}^h(\mathbf{x},t)$, as a function of both space and time, is discretized only in the space. Thus, Eq. (6) can be written as

$$\mathbf{u}^h(\mathbf{x},t)=\sum_{I=1}^{n}\phi_I(\mathbf{x})\mathbf{u}_I(t) \quad (26)$$

Substitution of Eq. (26) into the weak form (25) for all nodes leads to the following discretized system equation

$$\mathbf{M}\ddot{\mathbf{u}}(t)+\mathbf{C}\dot{\mathbf{u}}(t)+\mathbf{K}\mathbf{u}(t)=\mathbf{f}(t) \quad (27)$$

where $\mathbf{M}$, $\mathbf{C}$, $\mathbf{K}$, and $\mathbf{f}$ are the matrices of mass, damping, stiffness and force, respectively. They are the following forms

$$\mathbf{M}_{IJ}=\sum_{i=1}^{M}\int_{T_{iI}}\rho N_I\mathbf{\Phi}_J\mathrm{d}\Omega \quad (28a)$$

$$\mathbf{C}_{IJ}=\sum_{i=1}^{M}\int_{T_{iI}}cN_I\mathbf{\Phi}_J\mathrm{d}\Omega \quad (28b)$$

$$\mathbf{K}_{IJ}=\sum_{i=1}^{M}\int_{T_{iI}}\mathbf{V}_I^T\mathbf{D}\mathbf{B}_J\mathrm{d}\Omega \quad (28c)$$

$$\mathbf{f}_I(t)=\int_{\Gamma_{st}}N_I\bar{\mathbf{t}}(t)\mathrm{d}\Gamma+\sum_{i=1}^{M}\int_{T_{iI}}N_I\mathbf{b}(t)\mathrm{d}\Omega \quad (28d)$$

where the matrices of $\mathbf{D}$, $\mathbf{V}_I$, $\mathbf{B}_J$ and $\mathbf{\Phi}_J$ are defined in Eqs. (22a) $\sim$ (22d).

There are many time integration procedures for the solution of the equilibrium Eq. (27). In the present work we have used the Newmark method [Petyt (1990)] which is a generalization of the linear acceleration method. The Newmark method is an implicit time integration method and can give good results with respect to stability and accuracy. In this method the following assumptions are used

$$\dot{\mathbf{u}}_{t+\Delta t}=\dot{\mathbf{u}}_t+[(1-\delta)\ddot{\mathbf{u}}_t+\delta\ddot{\mathbf{u}}_{t+\Delta t}]\Delta t \quad (29a)$$

$$\mathbf{u}_{t+\Delta t}=\mathbf{u}_t+\dot{\mathbf{u}}_t\Delta t+[(\frac{1}{2}-\alpha)\ddot{\mathbf{u}}_t+\alpha\ddot{\mathbf{u}}_{t+\Delta t}]\Delta t^2 \quad (29b)$$

where α and δ are the parameters that can be determined to obtain integration stability and accuracy. The Newmark method is unconditionally stable provided

$$\delta\geq 0.5 \text{ and } \alpha\geq 0.25(0.5+\delta)^2 \quad (30)$$

In addition to (28a) and (28b), for solution of the displacements, velocities and accelerations at time $(t+\Delta t)$, the equilibrium Eq. (27) at time $(t+\Delta t)$ is also considered:

$$\mathbf{M}\ddot{\mathbf{u}}_{t+\Delta t}+\mathbf{C}\dot{\mathbf{u}}_{t+\Delta t}+\mathbf{K}\mathbf{u}_{t+\Delta t}=\mathbf{f}_{t+\Delta t} \quad (31)$$

Solving from Eq. (28b) for $\ddot{\mathbf{u}}_{t+\Delta t}$ in term of $\mathbf{u}_{t+\Delta t}$ and then substituting for $\ddot{\mathbf{u}}_{t+\Delta t}$ into Eq. (28a), we obtain equations for $\ddot{\mathbf{u}}_{t+\Delta t}$ and $\dot{\mathbf{u}}_{t+\Delta t}$, each in terms of the unknown displacements $\mathbf{u}_{t+\Delta t}$ only. These two relations for $\dot{\mathbf{u}}_{t+\Delta t}$ and $\ddot{\mathbf{u}}_{t+\Delta t}$ are substituted into Eq. (30) to solve for $\mathbf{u}_{t+\Delta t}$, after which, using Eq. (28a) and Eq. (28b), $\ddot{\mathbf{u}}_{t+\Delta t}$ and $\dot{\mathbf{u}}_{t+\Delta t}$ can also be calculated.

4 Numerical examples

This section presents the numerical studies dealing with the applications of the present MLNNI method for free and forced vibration analyses under plane stress conditions. Except specially mentioned, three Gaussian points are used in each Delaunay triangular region for domain integrals. The international standard unit system, namely, mass in kilograms, length in metres and time in seconds, is used for all the examples and thus no units are indicated with all the physical entities.

4.1 A Variable Cross-Section Beam

In the first example, a cantilever beam with variable cross-section shown in Figure 4 is analyzed. This problem has been studied using MLPG method by Gu and Liu (2001). The numerical parameters taken in the computation are: the length $L=10$m, the height $h(0)=5, h(L)=3$, the thickness $t=1.0$, Young's modulus $E=3.0\times10^7$, Poisson's ratio $v=0.3$ and mass density $\rho=1.0$.

The node discretization employed here is shown in Figure 5. To study the influence of number of Gaussian point on accuracy, six Gaussian points, as well as three Gaussian points, are used for domain integrals in each Delaunay triangular region. In Table 1, the MLNNI results are compared with those obtained by Gu and Liu (2001) and by FEM commercial software ABAQUS with very fine mesh (6282 DOF). From this table, one can observe that the computational results of the present MLNNI method are in good agreement with those obtained using MLPG and FEM methods. It can also be observed that the relative errors are almost on the same level when domain integrals are evaluated by using three and six Gaussian points in each Delaunay triangular region respectively. For the consideration of computational inefficiency, we recommend using three Gaussian points in each Delaunay triangular region for numerical integration in the present MLNNI method. The first four eigenmodes, obtained with the present MLNNI method using six Gaussian points in each Delaunay triangular region are plotted in Figure 6. Comparing with results obtained by the FEM commercial software ABAQUS, almost identical results of eigenmodes are obtained.

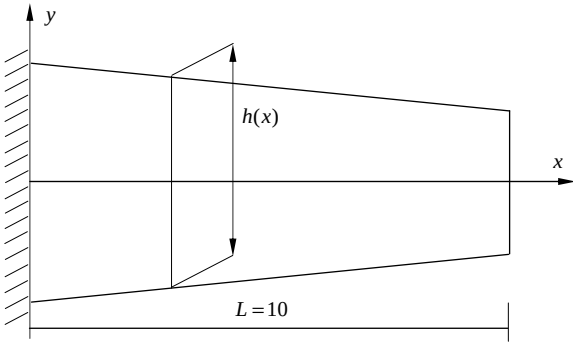

Figure 4: A variable cross-section beam

4.2 A Shear Wall With Four openings

The second numerical example regards a shear wall with four openings fixed at the two bottom edges, as shown in Figure 7. The free vibration is firstly studied here with Young's modulus $E = 10000$, Poisson's ratio $v = 0.2$, thickness

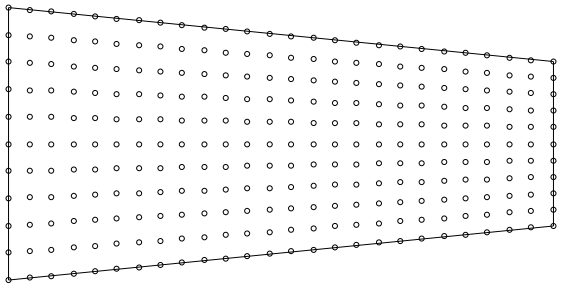

Figure 5: Node distribution for the variable cross-section beam

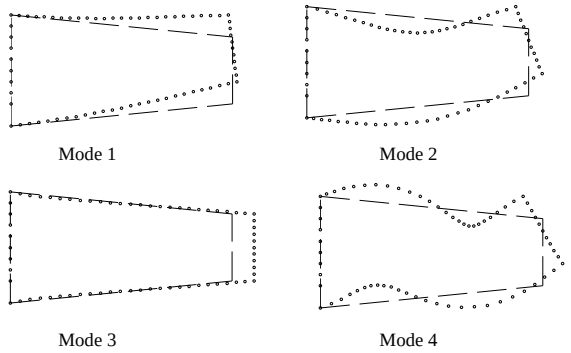

Figure 6: Eigenmodes for the variable cross-section beam by the MLNNI method

$t = 1$ and mass density $\rho = 1$. The free vibration of this shear wall was also analyzed by boundary element method [Brebbia, Telles and Wrobel (1984)] and meshless local Petrov-Galerkin method (MLPG) [Gu and Liu (2001)]. Both a regular node distribution and an irregular node distribution shown in Figure 8 are employed. Natural frequencies of the first eight modes are calculated by the present MLNNI method and listed in Table 2. It is evident that the results from the regular and irregular node distribution almost coincide with each other, and the results from both node distributions agree very well with those obtained by other methods.

The forced vibration is also studied here for this shear wall. The shear wall is subjected to a uniformly-distributed traction P in the form of a ramped wind load at the left face, as shown in Figure 7. This forced vibration problem has the same Young's modulus, Poisson's ratio, thickness and mass density as the free vibration problem of

Table 1: Natural frequencies of a variable cross-section beam

Mode	1	2	3	4	5
MLNNI (3 Gaussian points)	262.17	922.59	952.34	1867.78	2588.98
MLNNI (6 Gaussian points)	262.05	921.38	952.32	1863.72	2588.16
MLPG (Gu and Liu, 2001)	263.21	923.03	953.45	1855.14	2589.78
FEM (6282 DOF)	261.58	917.66	951.97	1852.28	2584.46

Table 2: Natural frequencies of a shear wall

Mode	MLNNI (regular)	MLNNI (irregular)	MLPG (Gu and Liu,2001)	BEM (Brebbia et al., 1984)
1	2.071	2.070	2.069	2.079
2	7.105	7.105	7.154	7.181
3	7.625	7.627	7.742	7.644
4	11.923	11.936	12.163	11.833
5	15.395	15.436	15.587	15.947
6	18.394	18.422	18.731	18.644
7	19.942	19.956	20.573	20.268
8	22.307	22.329	23.081	22.765

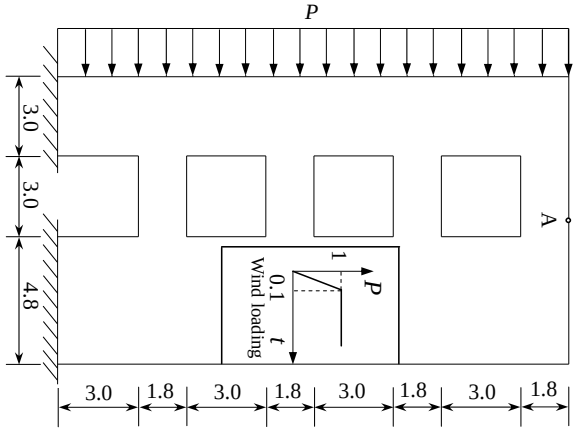

Figure 7: Geometry and loading of a shear wall with four openings

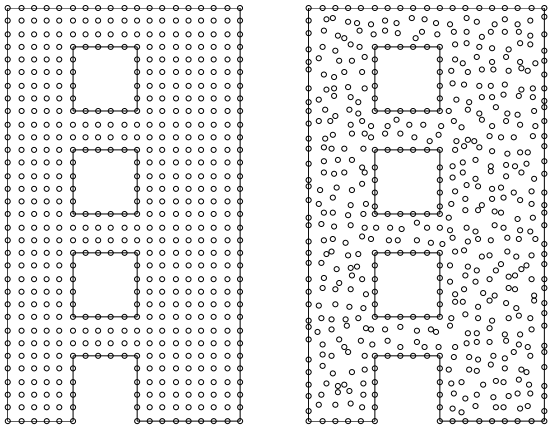

Figure 8: Node discretization for a shear wall with four openings: (a) regularly distributed 559 nodes; (b) irregularly distributed 559 nodes.

this example. The time step used in Newmark method is $\Delta t = 1 \times 10^{-3}$ and damping coefficient $c = 0$ is used. The results in terms of the history of the horizontal displacement of point A (5.4, 19.2) are compared with those obtained by the finite element software ABAQUS/Explicit and are given in Figure 9. The results corresponding to both the regular and irregular node distribution shown in Figure 8 are in good agreement with each other and with those of the finite element software ABAQUS. It can be easily found that the present MLNNI method works well for both free vibration analysis and forced vibration analysis. In addition, the numerical results also demonstrate that the irregular node distribution does not affect much the numerical accuracy in the present MLNNI method.

4.3 A Cantilever Beam

The forced vibration of a cantilever beam as shown in Figure 10 is modeled as the third exam-

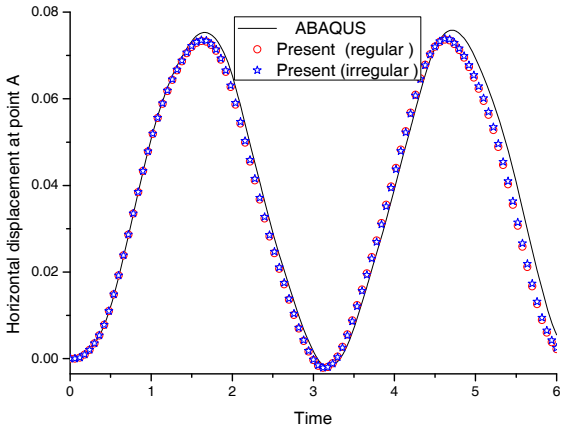

Figure 9: Horizontal displacement at point A under the ramped wind loading

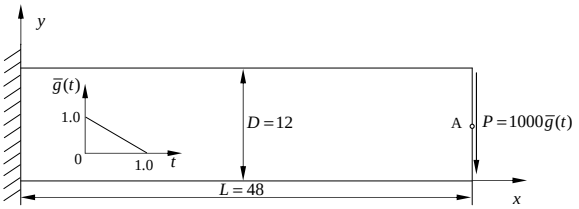

Figure 10: A cantilever beam for forced vibration and transient loading

ple. The numerical parameters taken in the computation are length $L = 48$, height $D = 12$, thickness $t = 1.0$, Young's modulus $E = 3.0 \times 10^7$, Poisson's ratio $v = 0.3$, and mass density $\rho = 1.0$. The beam is subjected to a transient parabolic traction at the free end, $P = 1000\overline{g}(t)$. $\overline{g}(t)$ is the function of time and is given in the following form

$$\overline{g}(t) = \begin{cases} 1-t, & 0 \le t \le 1 \\ 0, & t > 1 \end{cases} \tag{32}$$

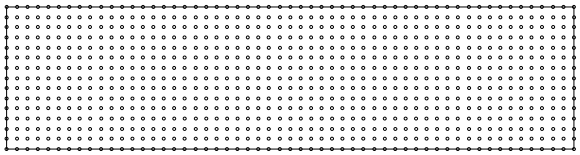

Figure 11: Node distribution for a cantilever beam

As shown in Figure 11, a regular node distribution with 825 nodes is employed here. The time step

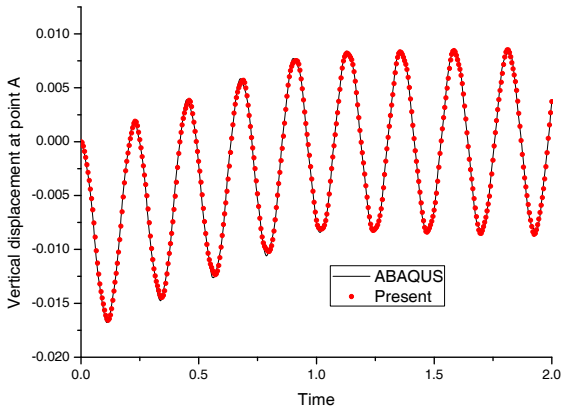

Figure 12: Vertical displacement at point A without damping under transient loading

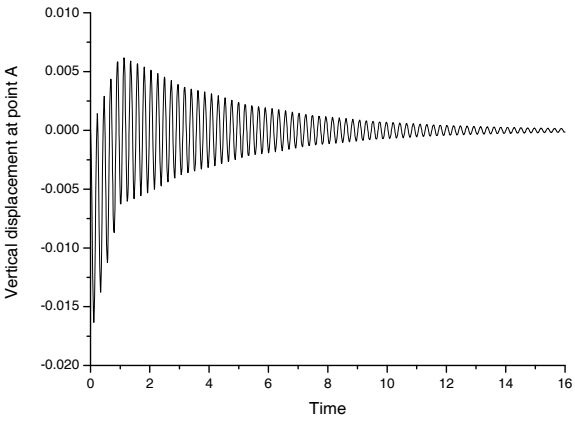

Figure 13: Vertical displacement at point A with damping under transient loading

used in Newmark method is $\Delta t = 5 \times 10^{-3}$. When the damping is neglected ($c = 0$), the computational results for the vertical displacement history at point A (48.0, 6.0) using the present MLNNI are graphed in Figure 12. For comparison, the results obtained by the finite element software, ABAQUS/Explicit, for the same point are also plotted in the same graph. The results are almost identical which proves the validity of the present method. The computational results with damping $c = 0.5$ are presented in Figure 13. One can observe from Figure 13 that the response is declined with time because of damping.

4.4 A Perforated Tension Strip

The last example is a perforated strip in axial tension as shown in Figure 14. The strip is subjected to a Heaviside tension step load with initial value $P = 7.5 \times 10^7$. The material properties of the strip are: Young's modulus $E = 2.1 \times 10^{11}$, Poisson's ratio $v = 0.3$, mass density $\rho = 7.85 \times 10^3$, and damping coefficient $c = 0$. This forced vibration problem has been studied using the dual reciprocity BEM by Kontoni and Beskos (1993). As can be seen from Figure 15, only the upper right quadrant of the strip is modeled due to the symmetry. Symmetry conditions are imposed on the left and bottom edges, and the inner boundary of the hole is traction free. The time step used in the Newmark time integration scheme is $\Delta t = 4 \times 10^{-7}$. Figures 16 and 17 depict the vertical displacement history of point A (0.00, 0.05) and the horizontal displacement history of point B (0.05, 0.00) respectively. Also shown in these Figures are the computational results obtained by the finite element software, ABAQUS/Explicit. It is evident that the results obtained by the present method are in very good agreement with those obtained using ABAQUS. Comparing the results here with those reported by Kontoni and Beskos (1993) also confirms the effectiveness and accuracy of the developed MLNNI method for forced vibration analysis.

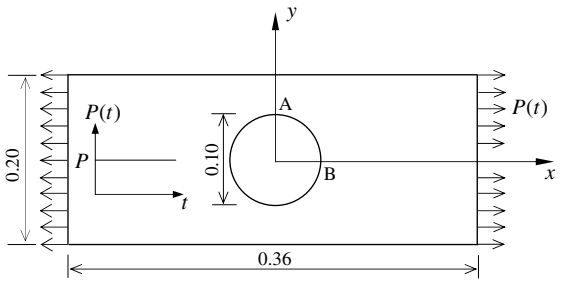

Figure 14: Geometry and loading of a perforated tension strip

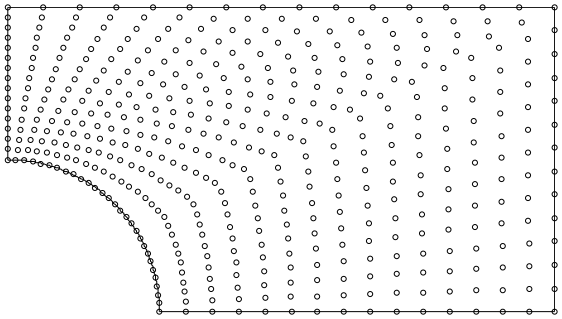

Figure 15: Node discretization for a perforated tension strip

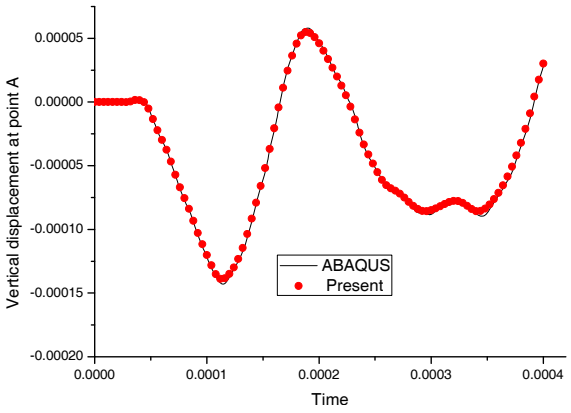

Figure 16: Vertical displacement at point A under the Heaviside loading

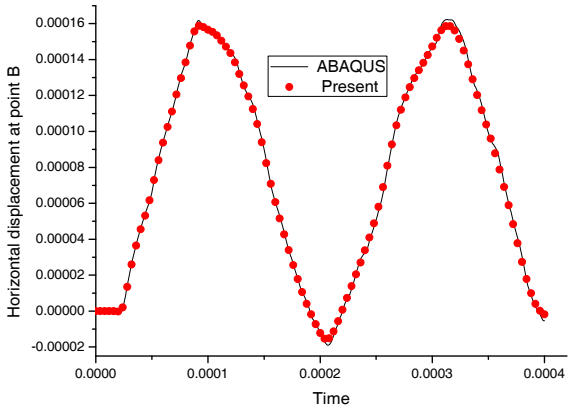

Figure 17: Vertical displacement at point B under the Heaviside loading

5 Conclusions

A meshless local natural neighbour interpolation (MLNNI) method has been developed for free and forced vibration analyses of two dimensional structures in this paper. This is an attempt to use the natural neighbour interpolation (NNI) in the generalized meshless local Petrov-Galerkin (MLPG) method. The local weak form of the dy-

namic partial differential equations is generated by using the local weighted residual method. The NNI and the three-node triangular FEM shape function are chosen differently as trial function and test function. Since the shape functions so formulated possess delta function property, the essential boundary conditions can be easily implemented. By virtue of the Delaunay tessellation, the construction of local subdomains is very simple for all nodes and domain integrals can be easily evaluated over included Delaunay triangles in each polygonal subdomain. Extensive structural dynamic analyses of four examples have been successfully carried out using the present MLNNI method. The fact that these examples have quite different dynamic behaviour, geometries, material properties, boundary conditions, demonstrates the high generality and wide applicability of the MLNNI method for structural dynamic analysis. In the next future a special attention will be devoted to develop the present MLNNI method for transient dynamic analysis of elastoplastic structures. This work is currently underway.

Acknowledgement: This paper was supported by the National Foundation for Excellent Doctoral Thesis of China (200025), the Program for New Century Excellent Talents in University (NCET-04-0075) and by the National Natural Science Foundation of China (19902007).

References

Atluri, S. N.; Kim, H. G.; Cho, J. Y. (1999): A critical assessment of the truly meshless local Petrov-Galerkin (MLPG) and local boundary integral equation (LBIE) methods. *Computational Mechanics*, Vol. 24, pp. 348-372.

Atluri, S. N.; Zhu, T. (1998): A new meshless local Petrov-Galerkin (MLPG) approach in computational mechanics. *Computational Mechanics*, Vol. 22, pp. 117-127.

Barry, W. (2004): A Wachspress meshless local Petrov-Galerkin method. *Engineering Analysis with Boundary Elements*, Vol. 28, pp. 509-523.

Belytschko, T.; Lu, Y. Y.; Gu, L. (1994): Element free Galerkin methods. *International Journal for Numerical Methods in Engineering*, Vol. 37, pp. 229-256.

Brebbia, C. A.; Telles, J. C. F.; Wrobel, L. C. (1984): *Boundary Element Techniques*, Springer-Verlag, Berlin.

Cai, Y. C.; Zhu, H. H. (2004): A meshless local natural neighbour interpolation method for stress analysis of solids. *Engineering Analysis with Boundary Elements*, Vol. 28, pp. 607-613.

Chen, S. S.; Liu, Y. H.; Cen, Z. Z. (2008): A combined approach of the MLPG method and nonlinear programming for lower-bound limit analysis. *CMES: Computer Modeling in Engineering & Sciences*, Vol. 28, no. 1, pp. 39-55.

De, S.; Bathe, K. J. (2000): The method of finite spheres. *Computational Mechanics*, Vol. 25, pp. 329-345.

Gingold, R. A.; Moraghan, J. J. (1977): Smoothed Particle hydrodynamics: theory and applications to non-spherical stars. *Monthly Notices of the Royal Astronomical Society*, Vol. 181, pp.375-389.

Green, P. J.; Sibson, R. R. (1978): Computing Dirichlet tessellations in the plane. *Computer Journal*, Vol. 21, pp. 168-173.

Gu, Y. T.; Liu, G. R. (2001): A meshless local Petrov-Galerkin (MLPG) method for free and forced vibration analyses for solids. *Computational Mechanics*, Vol. 27, pp. 188-198.

Han, Z. D.; Atluri, S. N. (2004): Meshless local Petrov-Galerkin (MLPG) approaches for solving 3D problems in elasto-statics. *CMES: Computer Modeling in Engineering & Sciences*, Vol. 6, no. 2, pp. 169-188.

Han, Z. D.; Liu, H. T.; Rajendran, A. M.; Atluri, S. N. (2006): The applications of meshless local Petrov-Galerkin (MLPG) approaches in high-speed impact, penetration and perforation problems. *CMES: Computer Modeling in Engineering & Sciences*, Vol. 14, no. 2, pp. 119-128.

Han, Z. D.; Rajendran, A. M.; Atluri, S. N. (2005): Meshless local Petrov-Galerkin (MLPG) approaches for solving nonlinear problems with

large deformation and rotation. *CMES: Computer Modeling in Engineering & Sciences*, Vol. 10, no. 1, pp. 1-12.

Johnson, J. N.; Owen, J. M. (2007): A meshless local Petrov-Galerkin method for magnetic diffusion in non-magnetic conductors. *CMES: Computer Modeling in Engineering & Sciences*, Vol. 22, no. 3, pp. 165-188.

Kontoni, D. P. N.; Beskos, D. E. (1993): Transient dynamic elastoplastic analysis by the dual reciprocity BEM. *Engineering Analysis with Boundary Elements*, Vol. 12, pp. 1-16.

Li, H.; Wang, Q. X.; Lam, K. Y. (2004): Development of a novel meshless Local Kriging (LoKriging) method for structural dynamic analysis. *Computer Methods in Applied Mechanics and Engineering*, Vol. 193, pp. 2599-2619.

Liu, G. R.; Gu, Y. T. (2001): A local radial point interpolation method (LRPIM) for free vibration analyses of 2-D solids. *Journal of Sound and Vibration*, Vol. 246, no. 1, pp. 29-46.

Liu, W. K.; Jun, S.; Zhang, Y. F. (1995): Reproducing kernel particle methods. *International Journal for Numerical Methods in Fluids*, Vol. 20, pp. 1081-1106.

Most, T. (2007): A natural neighbour-based moving least-squares approach for the element-free Galerkin method. *International Journal for Numerical Methods in Engineering*, Vol. 71, pp. 224-252.

Petyt, M. (1990): *Introduction to finite element vibration analysis*. Cambridge University Press, Cambridge.

Sukumar, N.; Moran, B.; Belytschko, T. (1998): The natural element method in solid mechanics. *International Journal for Numerical Methods in Engineering*, Vol. 43, pp. 839-887.

Sukumar, N.; Moran, B.; Semenov, A. Yu.; Belikov, V. V. (2001): Natural neighbour Galerkin methods. *International Journal for Numerical Methods in Engineering*, Vol. 50, pp. 1-27.

Wang, K.; Zhou, S. J.; Shan, G. J. (2005): The natural neighbour Petrov-Galerkin method for elasto-statics. *International Journal for Numerical Methods in Engineering*, Vol. 63, pp. 1126-1145.

Xiao, J. R. (2004): Local Heaviside weighted MLPG meshless method for two-dimensional solids using compactly supported radial basis functions. *Computer Methods in Applied Mechanics and Engineering*, Vol. 193, pp.117-138.